

Towards automatizing detection and quantification of intestinal metaplasia: a multi-expert comparative study

Fabian Cano^{1,*}, Mauricio Caviedes¹, Andres Siabatto¹, Jesus Villarreal¹, Jose Quijano¹, Alvaro Bedoya⁵, Satish E. Viswanath⁴, Angel Cruz-Roa³, Fabio Gonzalez², and Eduardo Romero¹

¹Computer Imaging and Medical Applications Laboratory - Cim@lab, Universidad Nacional de Colombia, Bogotá D.C., Colombia

²Machine Learning, Perception and Discovery Lab - Mindlab, Universidad Nacional de Colombia, Bogotá D.C., Colombia

³GITECX Research Group & Automatic Data-driven Analytics Laboratory - AdaLab, Universidad de los Llanos, Meta, Colombia

⁴Department of Biomedical Engineering, Case Western Reserve University, Cleveland, United States

⁵Centro de Investigación de Enfermedades digestivas y nutricionales - CIEDYN, Hospital Universitario Departamental de Nariño, Pasto, Colombia

*Corresponding author: facanor@unal.edu.co

ABSTRACT

Current gastric cancer risk systems are prone to errors since they evaluate a visual estimation of intestinal metaplasia percentages to assign a risk. This study presents an automated method to detect and quantify intestinal metaplasia using deep learning models as well as a comparative analysis with visual estimations of three experienced pathologists. Gastric samples were collected from two different cohorts: 149 asymptomatic volunteers from a region with a high prevalence of GCa in Colombia and 56 patients from a third-level hospital. Deep learning models were selected and trained to classify intestinal metaplasia, and predictions were used to estimate the percentage of intestinal metaplasia and assign the risk score. Results were compared with independent blinded assessments performed by three experienced pathologists. The best-performing deep learning architecture classified intestinal metaplasia with F1-Score of 0.80 ± 0.01 and AUC of 0.91 ± 0.01 . Among pathologists, inter-observer agreement by a Fleiss's Kappa score ranged from 0.61 to 0.75. In comparison, agreement between the pathologists and the best-performing model ranged from 0.37 to 0.54. Deep learning models show potential to detect and quantify the percentage of intestinal metaplasia with greater precision and reproducibility than experienced pathologists. Likewise, estimated risk shows high inter-observer variability when visually assigning the intestinal metaplasia percentage.

Introduction

Gastric cancer (GCa) was the fifth most commonly diagnosed cancer and the fifth leading cause of cancer-related death worldwide in 2022¹. Approximately 90% of GCa cases were diagnosed as adenocarcinomas, from which the most common type was intestinal adenocarcinoma². The high mortality rate associated with GCa is closely related to asymptomatic progression, however, if diagnosed at early stages, patient survival improves considerably³. The way in which this cancer develops and progresses is not completely clear, probably a combination of genetic factors associated with bacterial aggressiveness, the *Helicobacter pylori*, and environmental or lifestyle factors⁴. Given the lack of effective strategies to cure GCa, early diagnosis remains the most promising strategy to reduce both incidence and mortality rates⁵.

Currently, the screening protocol is guided by the Sydney System, introduced in 1991⁶ and updated in 1994 as the Updated Sydney System (USS)⁷. This system recommends histological evaluation of at least five gastric biopsies obtained from both the antrum and corpus, three from lesser curvature and two from greater curvature. This biased estimator has been popularized in practice because the incisura angularis has been considered an area with higher risk and therefore has been included as an additional antrum biopsy⁸, and some studies have observed premalignant lesions in this region⁹. Overall, *Helicobacter pylori*, mononuclear cells, loss of glands (atrophy), intestinal metaplasia, inflammation or dysplasia can be found in any of the five collected biopsies. Particular attention has been paid to intestinal metaplasia which has been scored in different categories: 0 (absence), 1 (mild), 2 (moderate), and 3 (severe), a combination of the extent and topographic distribution of microscopic changes¹⁰. This type of lesion is considered a gastric adaptation to chronic infection with *Helicobacter pylori*¹¹ and a pivotal event in GCa progression,

described as a “*point of no return*”¹². The final step to establish a progression risk to GCa is to assign a stage¹³. Protocols developed to assign this risk are basically the Operative Link for Gastritis Assessment (OLGA) system¹⁴ and the Operative Link on Gastric Intestinal Metaplasia (OLGIM) system¹⁵ (specifically designed to stage the extent and distribution of intestinal metaplasia). Both systems classify patients from stage 0 (lowest risk) to stage IV (highest risk).

Recently, some concerns have been raised about the uncertainty and clinical implications of current gastric risk stratification^{16,17} after the original USS version was introduced. Several publications have reported variability among general pathologists when assigning OLGIM stages^{16,18,19} and they have documented that these systems may underestimate or overestimate cancer risk^{9,18,20}. Although some studies suggest that OLGIM may stratify GCa risk^{15,21}, there is currently no robust quantitative evidence to support this statement^{18,22}. Therefore, a more precise and reproducible method to quantify these premalignant lesions remains an unmet need¹⁶. In this context, automatic approaches are particularly appealing as they address many of the limitations associated with visual assessment. Deep learning, in particular, has demonstrated high accuracy for detecting and quantifying patterns in medical images¹⁶, with outstanding results reported in lung cancer^{23–25}, breast cancer^{26–28}, prostate cancer^{29–31}, and gastric cancer^{32–34}. Specifically in gastric cancer, deep learning models have shown improved diagnostic accuracy and reproducibility, while significantly reducing both inter- and intra-observer variability³⁵.

The current OLGIM risk assessment system, which routinely guides clinical decisions^{12,36}, assigns a risk score by heuristically combining visual estimations of intestinal metaplasia from five different gastric biopsy sites. In this context, intestinal metaplasia remains a critical premalignant GCa stage that requires accurate and reproducible quantification¹⁶. Interestingly, some studies have reported cases classified as OLGIM low-risk who were later diagnosed with gastric cancer^{22,37}, while others identified as high-risk never developed cancer and, in some cases, reversed the lesion^{38,39}. In summary, these investigations indicate that subjectively estimated GCa risk is prone to errors and expert-visually-dependent¹².

In this study, an automatic deep learning approach is proposed to accurately detect and quantify intestinal metaplasia in H&E-stained images. Specifically, the main contributions of this study are as follows:

- Accurate automatic quantification of the intestinal metaplasia percentage by applying and adapting a set of state-of-the-art neural networks.
- Comparison of state-of-the-art deep learning models and a foundational model against individual assessment performed by three experienced pathologists to estimate the intestinal metaplasia percentage in H&E-stained images.
- By testing with two independent cohorts, this investigation assesses model robustness and generalization.

The rest of this document is organized as follows: section *Methods* describes the proposed methodology, including datasets, deep learning models, automatic detection and scoring of intestinal metaplasia and evaluation criteria. Section *Results* presents the experimental results and their comparison with the expert assessments. Section *Discussion* provides a discussion of the findings, including their interpretation, limitations, and implications. Finally, section *Conclusion* summarizes conclusion of the study.

Methods

This study aims to evaluate automatic quantification of the intestinal metaplasia percentage using deep learning models and to compare these assessments with manual estimations of three experienced pathologists. Four state-of-the-art deep learning models, including a foundational model pre-trained in histopathology images, were fine-tuned and evaluated to classify image patches as positive or negative for intestinal metaplasia. Subsequently, predictions of the best-performing model were used to estimate the percentage of intestinal metaplasia and to assign a score for antrum and corpus gastric biopsies, as shown in Figure 1. These automatic assessments were then compared with manual estimations, followed by an inter-observer agreement analysis and quantification of the variability among pathologists.

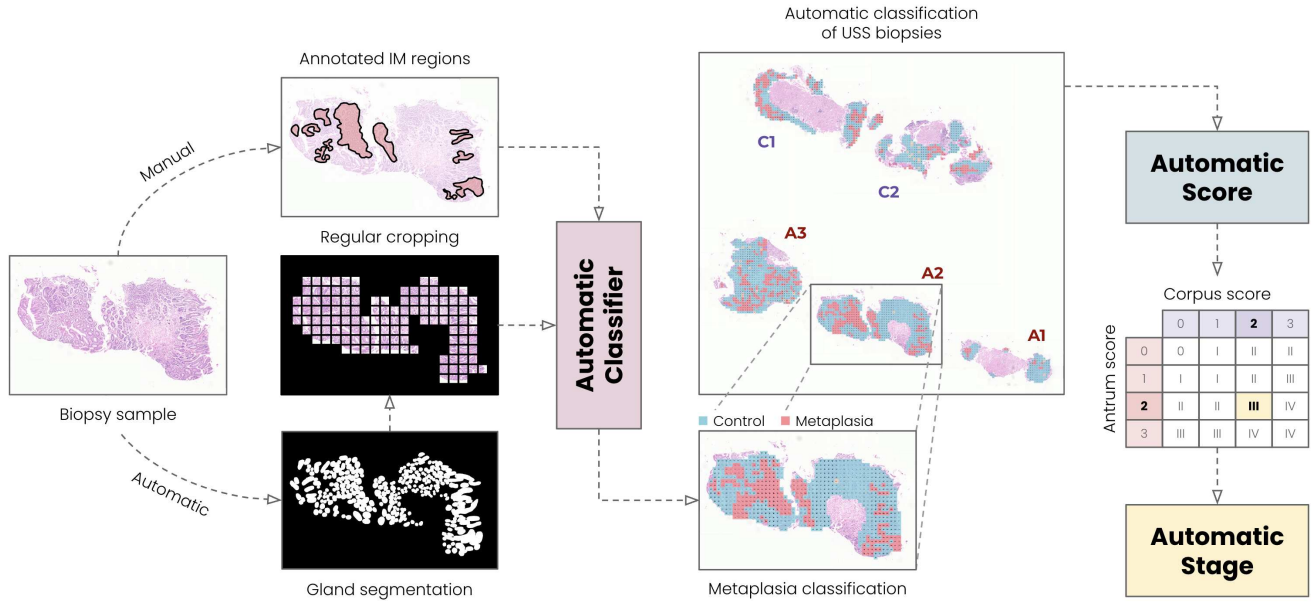


Figure 1. Proposed workflow of the automatic intestinal metaplasia classification with deep learning models and automatic scoring using the proportion of intestinal metaplasia in both antrum and corpus biopsies.

Gastric dataset and demographics

Gastric samples from two independent cohorts were digitized. The first cohort consists of 149 asymptomatic volunteers who were selected from an independent study provided by the *CIEDYN* foundation, a partner of the *Urkunina5000* project⁴⁰. This study performed an endoscopic and pathological characterization of gastric disease in 5.000 volunteers from 55 small villages in *Nariño*, Colombia, a region long observed as being GCa prevalent for the past two decades. Asymptomatic volunteers were men and women aged 30 – 70 years, who had lived in these areas for at least the last 10 years and had never undergone an endoscopy procedure, nor been diagnosed with GCa, any other type of cancer, or any known gastric pathology. The second cohort included 56 patients from the *Hospital Universitario Nacional de Colombia* included in a larger study which was approved by the ethics committee (Act No. 007, Apr 29 2022). Patients were men and women who present symptoms suggestive of gastritis or other forms of gastric discomfort. However, none of them had a previous GCa diagnosis or any other type of lesion.

Biopsy assessment

At least five gastric biopsies were obtained according to the USS (Fig. 2) in both cohorts. Specifically, two biopsies were taken from the antrum (A_1 , A_2) (the lesser and greater curvature, both within 2 cm to 3 cm far from the pylorus), two biopsies from the corpus (C_1 , C_2) (from the lesser curvature, approximately 4 cm proximal to the angle and from the middle portion of the greater curvature, about 8 cm from the cardias) and one biopsy from the incisura angularis (A_3) (antral-corpus transition zone). All biopsies were fixed in formalin and embedded in paraffin blocks, from which successive sections from the same case were stained with H&E.

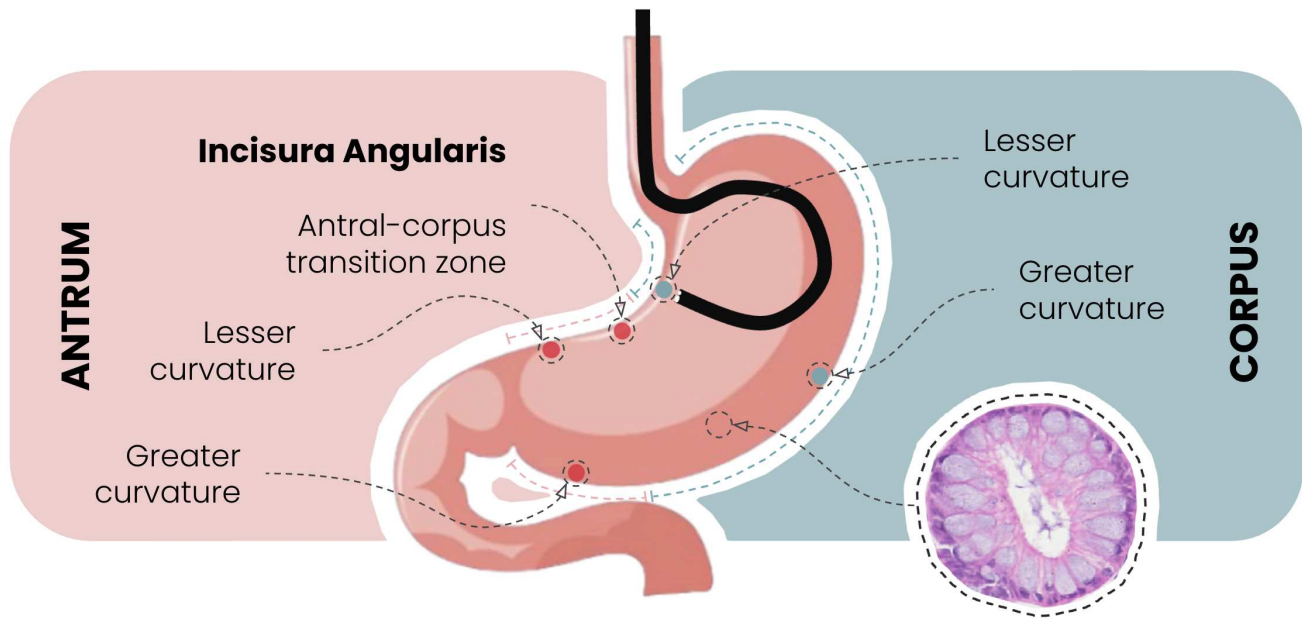


Figure 2. Biopsy places established for GCa detection according to the Updated Sydney System (USS). Antrum: Lesser curvature, Greater curvature and Antral-corporal transition zone (incisura angularis). Corpus: Lesser curvature and Greater curvature.

All cases were digitized using a whole-slide image (WSI) scanner (MoticEasyScan Pro), with a $\times 40$ objective, corresponding to a spatial resolution of $0.255 \mu\text{m}$ per pixel (MPP). Each case comprised five biopsies (one per anatomical region of the stomach), resulting in a total of 205 WSI, i.e., 149 from the first cohort and 56 from the second. The first cohort was used to train and evaluate the deep learning models including 73 cases for training, 32 cases for validation and 44 cases for testing. The second cohort was used exclusively as an external testing set.

Each case was independently assessed by three experienced pathologists following the Operative Link on Gastric Intestinal Metaplasia (OLGIM) system. This system assumes that variations regarding extent and topographical distribution of intestinal metaplasia reflect distinct clinic-pathological scenarios, each corresponding to a specific GCa risk. Pathologists performed blinded evaluations to estimate the proportion of intestinal metaplasia at five standardized biopsy sites: three from the mucosecreting area (two from the antrum and one from the incisura angularis) and two from the oxyntic mucosa (lesser and greater curvature of the corpus). After intestinal metaplasia was detected, a score was assigned as the estimated percentage of glands with goblet cells, ideally assessed in full-thickness (perpendicular) mucosa sections. Each biopsy was independently scored following a four-tier scale: absence of metaplasia = 0% (score 0), mild metaplasia = 1 – 30% (score 1), moderate metaplasia = 31 – 60% (score 2), and severe metaplasia = > 60% (score 3). The scores for the antral biopsies (A_1 , A_2 , A_3) and the corpus biopsies (C_1 , C_2) were averaged separately to obtain a composite score for each region. Finally, risk is determined by combining mean scores of the antrum and corpus, as illustrated in Fig. 2.

Manual annotations of intestinal metaplasia

All cases were manually annotated by the most experienced pathologist, basically delineating those regions affected by intestinal metaplasia. Overall, these regions contain not only glands with intestinal metaplasia but also a non-negligible amount of stroma and surrounding tissues. The pathologist manually annotated intestinal metaplasia regions using a custom web software developed as part of the *Program for the Early Detection of Premalignant Lesions and Gastric Cancer in urban, rural and dispersed areas in the Department of Nariño*, equipped with basic tools to annotate and visualize WSI. Annotations were saved according to the Web Annotation Data Model standard⁴¹.

Additionally, all cases were evaluated by the three pathologists, who independently estimated the percentage of intestinal metaplasia in both antrum and corpus biopsies using the previously described four-tier scale. Based on these estimations, each pathologist assigned an OLGIM stage per case, derived from the previously mentioned heuristic combination. This staging reflects the presumed risk of gastric cancer progression associated with the distribution and severity of intestinal metaplasia.

Automatic detection of glandular regions

The initial step to detect and quantify intestinal metaplasia involves automatic segmentation of gastric glands. In this study, gland segmentation was performed applying a U-Net architecture with a ResNet18 backbone⁴², originally trained to segment colorectal glands. It should be strengthened out that colorectal and gastric glands exhibit remarkable morphological similarities⁴³, particularly by the presence of goblet cells associated with intestinal metaplasia, which by definition corresponds to structural changes resembling those observed in colorectal tissue⁴⁴.

The model was pre-trained using a dataset comprising 165 fields of view extracted from 16 H&E-stained whole-slide images from the GlaS database (Gland Segmentation in Colon Histology Images Challenge)⁴². Since gastric and colorectal glands are alike, this architecture processed the 205 WSI from both gastric cohorts. To adapt the model to the gastric domain, the most experienced pathologist manually annotated 2,434 glands from 15 randomly selected cases, including both metaplastic and non-metaplastic glands. This annotated dataset was used to fine-tune the U-Net architecture, achieving a Dice Score of 0.77 ± 0.22 with a test subset of 730 glands, that is, glands not included in the training phase.

Since the objective of this study is not only to segment glands but also to detect and quantify intestinal metaplasia, the segmented glands were used to define glandular regions. These regions are basically bounding boxes surrounding groups of glands, within which a grid of fields of view is drawn.

Labeling automatically detected fields of view

Intestinal metaplasia regions, manually annotated by the most experienced pathologist, were superimposed onto the previously described grid of fields of view. Fields overlapping the annotated regions were labeled as intestinal metaplasia. Each of these fields of view corresponds to square patches of 256×256 pixels, extracted at $\times 40$ magnification. Regions outside the glandular region were excluded from the analysis.

The 149 cases from the first cohort were divided into training, validation, and internal testing sets, while the 56 cases from the second cohort were exclusively used as an external test set. In total, 476,351 fields of view were extracted, being 136,682 for training, 59,629 for validation, 89,945 for internal testing, and 190,095 for external testing.

Automatic classification of intestinal metaplasia

Deep learning models

Fields of view labeled as metaplasia or control classes were used to train and evaluate a set of state-of-the-art deep learning models. Specifically, four state-of-the-art convolutional neural networks pre-trained with the ImageNet dataset⁴⁵, ResNet50⁴⁶, DenseNet121⁴⁷ and ConvNeXtTiny⁴⁸, were adapted to classify microscopic gastric fields. ResNet50 demonstrated remarkable performance in intestinal metaplasia classification, with predictions closely matching the assessments of experienced pathologists⁴⁹. DenseNet121 was used as the basis to construct a specialized histopathology framework⁵⁰. ConvNeXtTiny has demonstrated superior performance at identifying anatomical regions of the stomach in endoscopic images⁵¹. Furthermore, a foundational model, UNI2-h⁵², pre-trained with TCGA⁵³, a large-scale histopathology image dataset, was used as a feature extractor for the classification of intestinal metaplasia.

Warm-up and fine-tuning

A multi-layer perceptron (MLP) was trained on top of each model to perform the classification of intestinal metaplasia. All models followed a two-stage training scheme consisting of a warm-up and fine-tuning phase. During the warm-up phase, the backbone of each model was frozen to preserve visual features learned from large datasets, such as ImageNet or TCGA. In this phase, only the MLP weights were updated. Subsequently, in the fine-tuning phase, selected layers of the pre-trained backbone were progressively unfrozen, enabling joint optimization of both the backbone and the classification head. Fine-tuning was performed with a lower learning rate to minimize overfitting and preserve the most relevant features of the original pretraining.

Hyper-parameter optimization

Each model was trained, validated and tested using the data partition presented in section *Biopsy assessment*, along with the corresponding fields of view described in section *Labeling automatically detected fields of view*. The architecture of each model integrated a MLP consisting of a sequential block composed of a dropout layer, a fully-connected layer, and a batch normalization layer, followed by an output layer with a *softmax* activation function. Model training followed a two-phase scheme (warm-up and fine-tuning), each consisting of thirty epochs. A hyper-parameter optimization process was performed to determine the optimal learning rate and dropout values, based in three independent experimental runs. During the warm-up phase, only the MLP was trained, while the

backbone of the pre-trained model remained frozen. In the subsequent fine-tuning phase, 80% of the pre-trained model layers remained frozen, while the remaining 20% (the deepest layers) were unfrozen and jointly optimized with the MLP to refine task-specific representations.

Data augmentation strategy

The previously presented resulting dataset is imbalanced, with an approximate ratio of 9:1, being the *metaplasia* class the minority. To address this imbalance, an online data augmentation strategy was implemented during training. This strategy involved applying symmetrical rotations of 90° increments along the horizontal axis to artificially increase sample diversity and mitigate overfitting. Furthermore, class weights were adjusted before training, assigning greater importance to the minority class (*metaplasia*) in the loss function to compensate for the skewed class distribution.

Automatic quantification and scoring of intestinal metaplasia

Automatic quantification of intestinal metaplasia was performed independently by the four deep learning architectures at the level of the pre-established fields of view. Each field of view was set to a probability value of class membership (i.e., *metaplasia* or *control*), and model performance was assessed using standard metrics: Accuracy, Precision, Recall, F1-Score and Area Under the ROC Curve (AUC).

These regional proportions were then used to determine an intestinal metaplasia score according to the OLGIM system, by averaging the scores from the three antrum biopsies (A_1 , A_2 , A_3) and the two corpus biopsies (C_1 , C_2). These scores reflect both the extent and topographic distribution of intestinal metaplasia, and were further used to assign the OLGIM stage by intersecting the antrum and corpus scores. Stages 0 - II were classified as low-risk, while stages III - IV were considered high-risk for GCa progression (Fig. 2).

Quantifying variability of manual and automatic estimations

Inter-observer variability

The 205 cases in both cohorts were independently evaluated by three experienced pathologists following the OLGIM system. Each pathologist estimated the extent of intestinal metaplasia in both antrum and corpus biopsies, assigning a score from 0 to 3. Based on these scores, an OLGIM stage was assigned: stages 0, I or II indicate the lowest risk, while stages III and IV indicate the highest risk. To assess inter-observer agreement, Fleiss' Kappa coefficient was calculated to measure overall consistency among the three pathologists, and Cohen's Kappa coefficient was used to assess pairwise agreement. Both metrics range from 0 (no agreement) to 1 (perfect agreement) with higher values indicating greater agreement.

Comparison between manual and automatic intestinal metaplasia percentages

Automatic scores calculated by the deep learning models were compared against the manual estimations provided by three experienced pathologists in two complementary approaches.

First, trends and variability of antrum and corpus intestinal metaplasia percentages are plotted to show differences between the three pathologists and four deep learning models. Second, a separate plot illustrates the distribution of the assigned OLGIM stages, allowing a direct comparison of staging variability between manual assessments and automated predictions.

Results

Automatic classification performance

Deep learning models were trained, validated and tested using the first cohort of 149 cases, and externally tested with the second, independent cohort of 56 cases. The classification results, summarized in Table 1, show mean and standard deviation for both internal and external test sets. These metrics were calculated across three experimental runs during the hyperparameter optimization phase and test sets were left aside from the beginning to ensure unbiased evaluation. Under these conditions, ConvNeXtTiny achieved the highest performance when classifying fields of view, with F1-Score 0.80 ± 0.01 , and AUC 0.91 ± 0.01 , for the internal test set, and F1-Score 0.73 ± 0.01 , and AUC 0.83 ± 0.01 for the external test set. The UNI2-h foundational model, currently considered a state-of-the-art architecture, showed the poorest performance for intestinal metaplasia classification with F1-Score 0.72 ± 0.01 and AUC 0.84 ± 0.01 , for the internal test set, and F1-Score 0.62 ± 0.01 and AUC 0.75 ± 0.01 for the external test set.

Table 1. Performance for the field-of-view-level classification models with the internal (1st cohort) and external (2nd cohort) testing sets.

Architecture	Precision	Sensitivity	F1-Score	AUC
Internal test				
ConvNeXtTiny	0.79 ± 0.01	0.80 ± 0.01	0.80 ± 0.01	0.91 ± 0.01
ResNet50	0.82 ± 0.01	0.77 ± 0.01	0.79 ± 0.01	0.90 ± 0.01
DenseNet121	0.83 ± 0.02	0.74 ± 0.03	0.77 ± 0.02	0.89 ± 0.01
UNI2-h	0.75 ± 0.02	0.70 ± 0.02	0.72 ± 0.01	0.84 ± 0.01
External test				
ConvNeXtTiny	0.78 ± 0.01	0.69 ± 0.01	0.73 ± 0.01	0.83 ± 0.01
ResNet50	0.80 ± 0.01	0.64 ± 0.01	0.68 ± 0.01	0.79 ± 0.01
DenseNet121	0.81 ± 0.04	0.64 ± 0.02	0.68 ± 0.01	0.82 ± 0.01
UNI2-h	0.81 ± 0.01	0.51 ± 0.02	0.62 ± 0.01	0.75 ± 0.01

Automatic quantification and scoring of intestinal metaplasia

The fields of view predicted by the best-performing model were superimposed to the corresponding whole-slide images of both cohorts. Predictions were plotted in a color-code map: blue and red, the ones correctly classified, and orange and purple, the misclassified ones (Fig. 3). These prediction maps highlight in red areas where the model agrees with the expert-annotated regions. Within these annotated regions, areas in purple correspond to those in which the model disagrees with the expert. Interestingly, the model also identifies metaplastic areas (in orange) that have not previously been annotated. In general, most misclassified fields of view were observed within large regions, which often contain a heterogeneous mix of metaplastic glands, control glands, stroma, and foveolar epithelium.

Quantifying variability of manual and automatic estimations

Results of the inter-observer agreement

Inter-observer agreement among pathologists and the best-performing deep learning model is presented in Figure 4. The Cohen’s Kappa coefficient shows pairwise inter-observer agreement in both the antrum and corpus, for both internal and external test sets. Given that experts provided an accurate estimation of the intestinal metaplasia percentage, manual-automatic comparison was performed at a finer level by binning the entire range into incremental intervals of 10%, i.e., ten intervals of 10% instead of the usual 0%, 30%, 60% and more. This uniform partition was used to evaluate agreement between manual and automated estimations. Fleiss’ Kappa, which measures overall agreement among all observers, indicated moderate agreement among the three pathologists, with scores of 0.31 for the antrum and 0.41 for the corpus. Overall, agreement between the deep learning model and individual pathologists was comparable to that observed between pairs of pathologists. The level of agreement obtained using the homogeneous partition was also consistent with previously reported OLGIM inter-observer agreement in the literature, with Fleiss’ Kappa scores of 0.48, indicating moderate agreement⁵⁴.

Subplots in Figure 5 show the inter-observer agreement among pathologists, as well as between the pathologists and the best-performing deep learning model, regarding the OLGIM staging. As previously reported in the literature⁵⁵, inter-observer agreement tends to increase when the categorical evaluation scale is simplified. In this work, expert agreement improved significantly when using a coarser grading scheme, the OLGIM staging system.

Variability of intestinal metaplasia percentages

Subplots in Figure 6 display box plots illustrating the relationship between the assigned intestinal metaplasia percentage (y-axis) and the corresponding OLGIM stage (x-axis), as determined by consensus among the three pathologists. As observed, expert variability is higher for intermediate stages, when compared with the other stages, probably because these stages are set by a higher number of antrum and corpus combinations, i.e., different OLGIM scores may produce the same stage. As expected, both manual and automatic estimations exhibit an increasing percentage trend of intestinal metaplasia with higher OLGIM stages. However, the automated model shows substantially lower variability across the four stages. As largely described in the literature, pathologists tend to overestimate the extent of the lesion¹⁸, typically assigning higher percentages compared to the automated model.

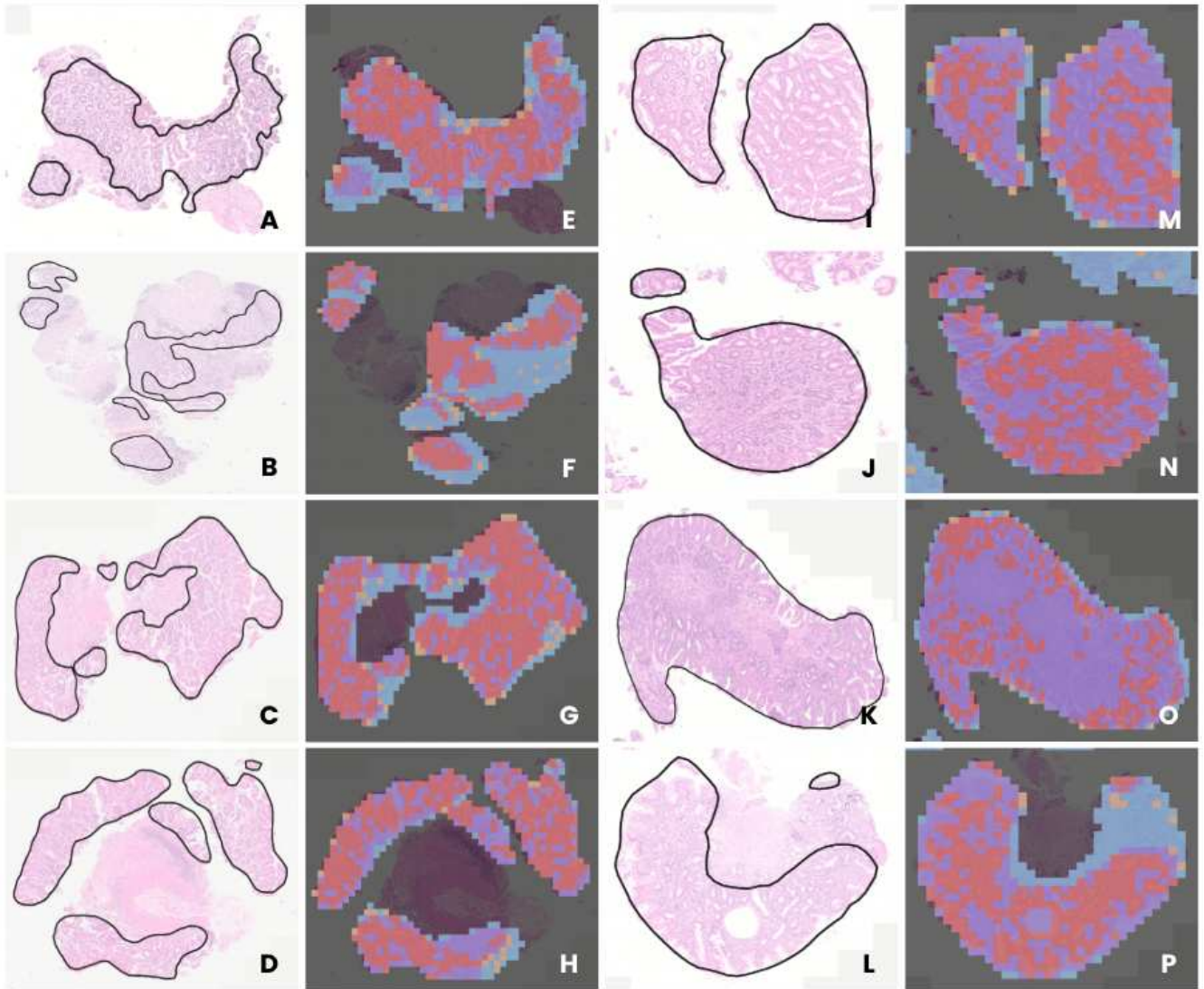


Figure 3. Comparison between annotated and automatically predicted regions. This visualization illustrates differences between regions annotated by the most experienced pathologist (A-D, for internal test samples, and I-L, for external test samples) with the prediction maps of the best performed model (E-H, for internal test samples, and M-P, for external test samples). Model predictions of fields of view are color-coded: correctly predicted as metaplastic are shown in red, and correctly predicted as control in blue. Control regions incorrectly predicted as metaplasia are displayed in orange and metaplastic regions incorrectly predicted as control in purple.

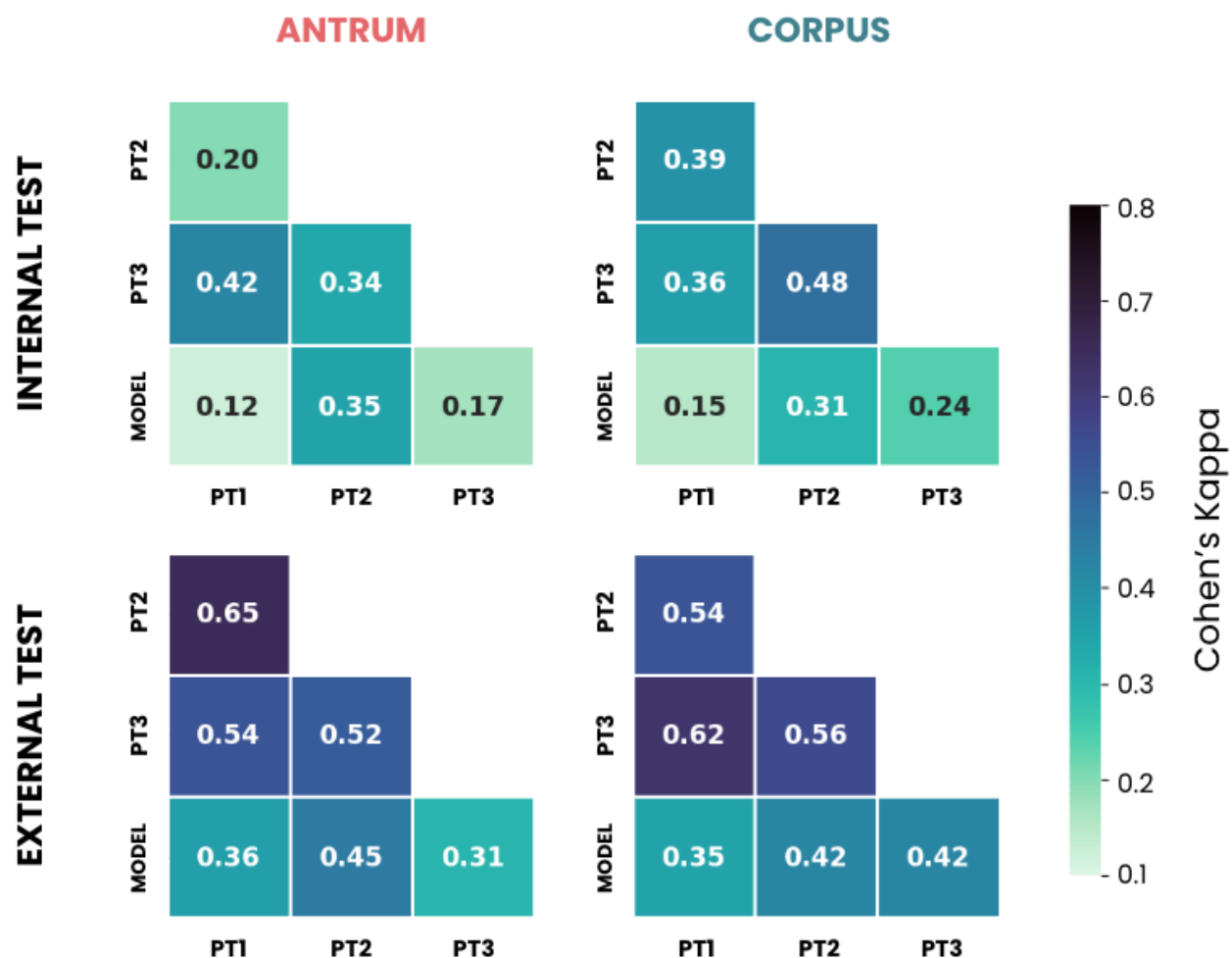


Figure 4. Inter-observer agreement among pathologists and the best-performing deep learning model for the internal and external test sets. PT1, PT2 and PT3 stand for the three pathologists, while MODEL refers to the best-performing automated model (ConvNeXtTiny). Subplots in the first column show agreement for the antrum, and subplots in the second column correspond the corpus.

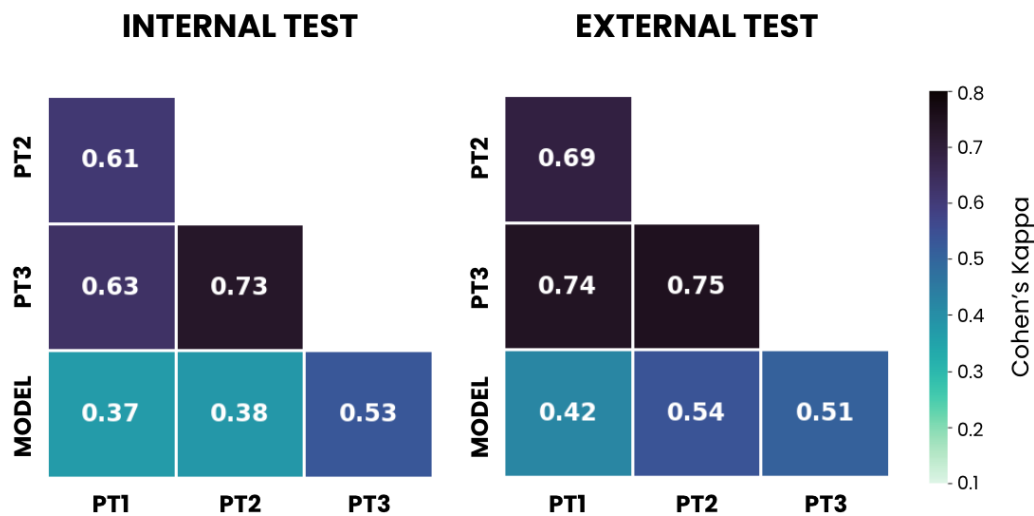


Figure 5. Inter-observer agreement compared with the automatic OLGIM staging on the internal and external test datasets.

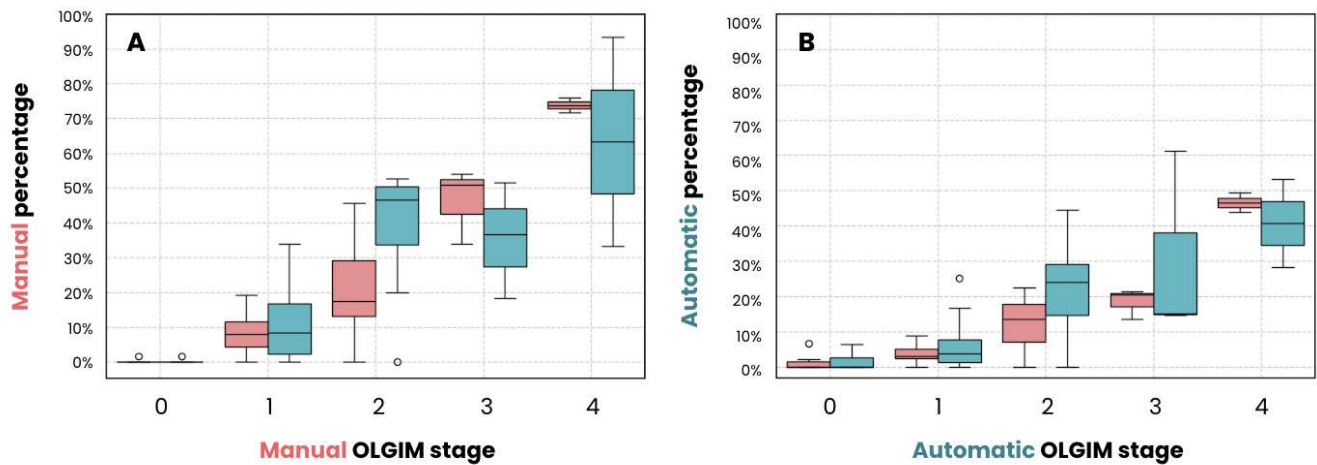


Figure 6. Distribution of manual (left) and automatic (right) intestinal metaplasia percentages in the antrum (red) and corpus (green), related to the consensus OLGIM stage assigned by pathologists.

Discussion

This paper has investigated the role of state-of-the-art deep learning models to detect and quantify intestinal metaplasia. Evaluation of these models has demonstrated remarkable performance for computing stroma, glands and the percentage of actual intestinal metaplasia. However, estimation of the OLGIM score is still a bottleneck since pathologists show high variability at estimating the intestinal metaplasia percentage, a result consistent with publications which have shown and discussed OLGIM limitations^{16,18,20}. As inferred from the presented results, decision uncertainty is still too high as to conclude that OLGIM should be the only element at managing and assigning a level of risk.

Several studies have investigated OLGIM limitations, among them the most important is the difficulty to report, i.e., many pathologists worldwide hardly report OLGIM stages since they are aware of the conflict introduced by the typical disagreement¹⁶, a moderate agreement is widely acknowledged^{54,56}. An inevitable criticism to OLGIM score is that this is by nature biased since intermediate stages are obtained with a higher number of combinations and therefore these stages are the more frequent, in other words dices are charged and as a result the confidence in this assessment ends up by being undermined.

Recent studies have demonstrated the effectiveness of deep learning models at classifying and grading pathologies in H&E images^{24,27,32}. Typically, the pathologist knowledge, the ground truth⁵⁷, consists in a set of delineated regions which serve to train models that closely replicate these visual annotations. However, the variable biology along with a subjective judgment, inevitably introduces additional biases. As a general rule, artificial intelligence models are good if data is available in the needed quantity and quality⁵⁸. However, annotations are an actual bottleneck since they are typically closed regions which include not only metaplasia, but in a great proportion stroma and normal glands⁵⁹. The agreements obtained here between experts and model predictions suggest further limitations: while models perform well at identifying regions with intestinal metaplasia and at estimating percentage, agreement with experts remains low, as reported in other publications⁵⁴. Nevertheless, the larger expert variability at estimating percentages when comparing with models is likely compensated by experience, a probable explanation of the OLGIM overestimation herein observed, and a result again consistent with studies in the literature about OLGIM limitations^{16,18}.

Despite the multifocal nature of the intestinal metaplasia, i.e. spreading along stomach regions, estimation of this condition considers this phenomenon as a binary problem: presence or absence. Both intestinal metaplasia extension and topographic distribution have been at the very base of risk estimation to progress, yet Correa et al. had already questioned this description because intestinal metaplasia is a mixture of morphological expressions of the different mucin enzymes associated to two main subtypes, complete and incomplete¹⁰. While complete metaplasia is characterized by the tissue resemblance to the small intestine with enterocytes displaying the brush border, the incomplete metaplasia is close to the colonic epithelium with multiple and irregular intra-cytoplasmic mucin droplets of variable size. Current estimation of metaplasia is still far from quantifying this level of detail, but clearly these AI tools may build a continuous description of the phenomenon instead of the limited binary characterization so far applied. In the present study deep learning models ended up by describing metaplasia as a binary phenomenon, aiming to drive any pattern to any of these two classes but with a variable uncertainty introduced by the presence of different morphological expressions of metaplasia. Consequently, these models could quantify not only the metaplasia presence/absence but also a continuous characterization of the lesion profiles, a necessary step towards a reproducible quantification and a personalized risk estimation.

Conclusion

Machine learning models demonstrate to accurately quantify the intestinal metaplasia proportion. Likewise, the model is clearly reproducible and introduces an objective factor in the chain of events leading to estimate the risk.

Author contributions

Conceptualization: FC, ACR, FG and ER; Data curation: FC, MC, AS, JV and JQ; Methodology: FC, MC, ACR, FG and ER; Formal analysis: FC, ACR, FG and ER; Writing - original draft preparation: FC and ER; Writing - review and editing: FC, ACR, FG and ER; Funding acquisition: ACR and ER; Resources: ACR, FG and ER; Supervision: FG and ER; Project administration: ER. All authors have read and agreed to the published version of the manuscript.

Funding

This work was partially supported by the project with code 110192092345 *Program for the Early Detection of Premalignant Lesions and Gastric Cancer in urban, rural and dispersed areas in the Department of Nariño* of call

No. 920 of 2022 of MinCiencias. This work was partially supported by project 52895, titled *Proposal for the strategic plan for the establishment of the Center of Excellence (Inter-Sites) in Medicine and Artificial Intelligence (SemAI)*, from the National Call for Proposals Bank for the Consolidation of Centers of Excellence 2020-2021 at *Universidad Nacional de Colombia*. This work was partially supported by project BPIN 2019000100060 *Implementation of a Network for Research, Technological Development and Innovation in Digital Pathology (RedPat) supported by Industry 4.0 technologies* from FCTel of SGR resources, which was approved by OCAD of FCTel and MinCiencias.

Acknowledgements

Special thanks to the CIEDYN foundation and the project BPIN 20150000100064 Urkunina5000, from which whole slides of gastric tissue were recovered from asymptomatic volunteers and subsequently digitized to be used in the development of this work.

Data availability

Internal and external data are publicly available at Harvard Dataverse⁶⁰.

Declarations

Conflict of interest

All authors declare no conflicts of interest.

Ethical considerations

This research study was conducted retrospectively using data provided by the CIEDYN foundation, a partner of the Urkunina5000 project, which contains information on ethical considerations in compliance with the Declaration of Helsinki. All patients signed informed consent forms. Additional ethics considerations was not required.

Informed consent

All asymptomatic volunteers selected for this study signed informed consent and all guarantees of anonymization were applied to their data.

References

1. Bray, F. *et al.* Global cancer statistics 2022: GLOBOCAN estimates of incidence and mortality worldwide for 36 cancers in 185 countries. *CA: a cancer journal for clinicians*. **74(3)**, 229–263 (2022).
2. Ajani, J. *et al.* Gastric adenocarcinoma. *Nat. Rev. Dis. Prim.* **3**, 1–19 (2017).
3. Tan, P. & Yeoh, K. Genetics and molecular pathogenesis of gastric adenocarcinoma. *Gastroenterology*. **149**, 1153–1162 (2015).
4. Puculek, M. *et al.* Helicobacter pylori associated factors in the development of gastric cancer with special reference to the early-onset subtype. *Oncotarget*. **9(57)**, 31146–31162 (2018).
5. Cai, Q. *et al.* Development and validation of a prediction rule for estimating gastric cancer risk in the Chinese high-risk population: a nationwide multicentre study. *Gut*. **68(9)**, 1576–1587 (2019).
6. Misiewicz, J. The Sydney System: a new classification of gastritis. Introduction. *J. Gastroenterol. Hepatol.* **6(3)**, 207–208 (1991).
7. Dixon, M. *et al.* Classification and grading of gastritis. The updated Sydney System. International Workshop on the Histopathology of Gastritis, Houston 1994. *Am. J. Surg. Pathol.* **20**, 1161–1181 (1996).
8. Rugge, M. *et al.* Gastritis staging in clinical practice: the olga staging system. *Gut*. **56(5)**, 631–636 (2007).
9. Crafa, P. *et al.* From Sidney to OLGA: an overview of atrophic gastritis. *Acta. Biomed.* **89(8-S)**, 93–99 (2018).
10. Correa, P. Gastric cancer: overview. *Gastroenterol. clinics North Am.* **42(2)**, 211–217 (2013).
11. Koulis, A. *et al.* Premalignant lesions and gastric cancer: Current understanding. *World J. Gastrointest. Oncol.* **11(9)**, 665–678 (2019).
12. Tjandra, D. *et al.* Gastric Intestinal Metaplasia: Challenges and the Opportunity for Precision Prevention. *Cancers*. **15**, 3913 (2023).
13. Marcos, P. *et al.* Endoscopic grading of gastric intestinal metaplasia on risk assessment for early gastric neoplasia: can we replace histology assessment also in the west? *Gut*. **69(10)**, 1762–1768 (2020).

14. Rugge, M. & Genta, R. Staging and grading of chronic gastritis. *Hum. Pathol.* **36**(3), 228–233 (2005).
15. Capelle, L. *et al.* The staging of gastritis with the OLGA system by using intestinal metaplasia as an accurate alternative for atrophic gastritis. *Gastrointest. Endosc.* **71**(7), 1150–1158 (2010).
16. Fang, S. *et al.* Diagnosing and grading gastric atrophy and intestinal metaplasia using semi-supervised deep learning on pathological images: development and validation study. *Gastric Cancer.* **27**, 343–354 (2024).
17. Zhao, Q. *et al.* Deep learning model can improve the diagnosis rate of endoscopic chronic atrophic gastritis: a prospective cohort study. *BMC Gastroenterol.* **22**(1), 133 (2022).
18. Yue, H. *et al.* The significance of OLGA and OLGIM staging systems in the risk assessment of gastric cancer: a systematic review and meta-analysis. *Gastric Cancer.* **21**, 579–587 (2018).
19. Isajevs, S. *et al.* Gastritis staging: interobserver agreement by applying OLGA and OLGIM systems. *Virchows. Arch.* **464**, 403–407 (2014).
20. Molaei, M. *et al.* Gastric atrophy: use of OLGA staging system in practice. *Gastroenterol. Hepatol. Bed. Bench.* **9**(1), 25–29 (2016).
21. Rugge, M. *et al.* Gastritis OLGA-staging and gastric cancer risk: a twelve-year clinicopathological followup study. *Aliment. Pharmacol. Ther.* **31**, 1104–1111 (2010).
22. Mansour-Ghanaei, F. *et al.* OLGA- and OLGIM-Based Staging in the Patients with Gastritis and Endoscopy Indications. *Turk. J. Gastroenterol.* **33**(2), 95–102 (2022).
23. Chen, C. *et al.* An annotation-free whole-slide training approach to pathological classification of lung cancer types using deep learning. *Nat. Commun.* **12**, 1193 (2021).
24. Coudray, N. *et al.* Classification and mutation prediction from non-small cell lung cancer histopathology images using deep learning. *Nat. Med.* **24**, 1559–1567 (2018).
25. Kanavati, F. *et al.* Weakly-supervised learning for lung carcinoma classification using deep learning. *Sci. Rep.* **10**, 9297 (2020).
26. Cruz-Roa, A. *et al.* High-throughput adaptive sampling for whole-slide histopathology image analysis (HASHI) via convolutional neural networks: Application to invasive breast cancer detection. *PLoS ONE.* **13**(5), e0196828 (2018).
27. Liu, M. *et al.* A Deep Learning Method for Breast Cancer Classification in the Pathology Images. *IEEE J. Biomed. Heal. Informatics.* **26**(10), 5025–5032 (2022).
28. Wetstein, S. *et al.* Deep learning-based breast cancer grading and survival analysis on whole-slide histopathology images. *Sci. Rep.* **12**, 15102 (2022).
29. Nir, G. *et al.* Automatic grading of prostate cancer in digitized histopathology images: Learning from multiple experts. *Med. Image. Anal.* **50**, 167–180 (2018).
30. Li, Y. *et al.* Automated Gleason Grading and Gleason Pattern Region Segmentation Based on Deep Learning for Pathological Images of Prostate Cancer. *IEEE Access.* **8**, 117714–117725 (2020).
31. Tolkach, Y. *et al.* High-accuracy prostate cancer pathology using deep learning. *Nat. Mach. Intell.* **2**, 411–418 (2020).
32. Wang, X. *et al.* Predicting gastric cancer outcome from resected lymph node histopathology images using deep learning. *Nat. Commun.* **12**, 1637 (2021).
33. Huang, B. *et al.* Accurate diagnosis and prognosis prediction of gastric cancer using deep learning on digital pathological images: A retrospective multicentre study. *EBioMedicine.* **73**, 103631 (2021).
34. Sharma, H. *et al.* Deep convolutional neural networks for automatic classification of gastric carcinoma using whole slide images in digital histopathology. *Comput. Med. Imaging. Graph.* **61**, 2–13 (2017).
35. Veldhuizen, G. P. *et al.* Deep learning-based subtyping of gastric cancer histology predicts clinical outcome: a multi-institutional retrospective study. *Gastric Cancer.* **26**(5), 708–720 (2023).
36. White, J. *et al.* Identifying the pre-malignant stomach: from guidelines to practice. *Transl. Gastroenterol. Hepatol.* **7**, 8 (2022).

37. Pimentel-Nunes, P. *et al.* Management of epithelial precancerous conditions and lesions in the stomach (MAPS II): European Society of Gastrointestinal Endoscopy (ESGE), European Helicobacter and Microbiota Study Group (EHMSG), European Society of Pathology (ESP), and Sociedade Portuguesa de Endoscopia Digestiva (SPED) guideline update 2019. *Endoscopy*. **51**, 365–388 (2019).
38. Hwang, Y. *et al.* Reversibility of atrophic gastritis and intestinal metaplasia after helicobacter pylori eradication — A prospective study for up to 10 years. *Aliment. Pharmacol. Ther.* **47**, 380–390 (2018).
39. Aumpan, N. *et al.* Predictors for regression and progression of intestinal metaplasia (IM): A large population-based study from low prevalence area of gastric cancer (IM-predictor trial). *PLoS One*. **16**(8), e0255601 (2021).
40. Bedoya, A. *et al.* Proyecto Urkunina 5000. Investigación de la prevalencia de lesiones precursoras y del efecto de la erradicación de *Helicobacter pylori* como prevención primaria del cáncer gástrico en el departamento de Nariño. *Rev. Colomb. Cir.* **33**(4), 345–352 (2019).
41. Sanderson, R. *et al.* Web Annotation Data Model: W3C Recommendation 23 February 2017. In *Proc. 5th Annu. ACM Web Sci. Conf.* 366–375 (2013).
42. Sirinukunwattana, K. *et al.* Gland segmentation in colon histology images: The glas challenge contest. *Med. image analysis*. **35**, 489–502 (2017).
43. Jass, J. Classification of colorectal cancer based on correlation of clinical, morphological and molecular features. *Histopathology* **50**(1), 113–130 (2007).
44. Shah, S. C. *et al.* Histologic subtyping of gastric intestinal metaplasia: overview and considerations for clinical practice. *Gastroenterology* **158**(3), 745–750 (2020).
45. Deng, J. *et al.* Imagenet: A large-scale hierarchical image database. In *2009 IEEE conference on computer vision pattern recognition*. 248–255 (2009).
46. He, K. *et al.* Deep residual learning for image recognition. *2016 IEEE Conf. on Comput. Vis. Pattern Recognit. (CVPR)*. 770–778 (2016).
47. Huang, G. *et al.* Densely connected convolutional networks. In *Proc. IEEE conference on computer vision pattern recognition* 4700–4708 (2017).
48. Liu, Z. *et al.* A convnet for the 2020s. In *Proc. IEEE/CVF conference on computer vision pattern recognition* 11976–11986 (2021).
49. Caviedes, M. *et al.* An automatic classification of metaplasia in gastric histopathology images. *2023 19th Int. Symp. on Med. Inf. Process. Analysis (SIPAIM)*. 1–4 (2023).
50. Riasatian, A. *et al.* Fine-tuning and training of densenet for histopathology image representation using tcga diagnostic slides. *Med. image analysis*. **70**, 102032 (2021).
51. Bravo, D. *et al.* Automatic Classification of Esophagogastrroduodenoscopy Sub-Anatomical Regions. *2023 IEEE 20th Int. Symp. on Biomed. Imaging (ISBI)*. 1–5 (2023).
52. Chen, R. J. *et al.* Towards a general-purpose foundation model for computational pathology. *Nat. Med.* **30**, 850–862 (2024).
53. Tomczak, K. *et al.* The cancer genome atlas (tcga): an immeasurable source of knowledge. *Contemp Oncol (Pozn)*. **19**(1A), A68–77 (2015).
54. Lerch, J. M. *et al.* Subtyping intestinal metaplasia in patients with chronic atrophic gastritis: an interobserver variability study. *Pathology*. **54**(3), 262–268 (2022).
55. Cross, S. S. Grading and scoring in histopathology. *Histopathology*. **33**(2), 99–106 (1998).
56. Salazar, B. *et al.* The OLGA-OLGIM staging and the interobserver agreement for gastritis and preneoplastic lesion screening: a cross-sectional study. *Virchows Arch.* **480**, 759–769 (2022).
57. Janowczyk, A. & Madabhushi, A. Deep learning for digital pathology image analysis: A comprehensive tutorial with selected use cases. *J. pathology informatics*. **7**(1), 29 (2016).
58. Vali-Betts, E. *et al.* Effects of image quantity and image source variation on machine learning histology differential diagnosis models. *J. Pathol. Informatics*. **12**(1), 5 (2021).
59. Selvaraju, R. *et al.* Grad-CAM: Visual Explanations From Deep Networks via Gradient-Based Localization. *Proc. IEEE Int. Conf. on Comput. Vis. (ICCV)*, 2017. 618–626 (2017).

60. Cano, F. & others. Replication data for: Towards automatizing detection and quantification of intestinal metaplasia: A multi-expert comparative study. *Harvard Dataverse* <https://doi.org/10.7910/DVN/NVUCW8> (2025).